Ion mobility mass spectrometry unveils global protein conformations in response to conditions that promote and reverse liquid-liquid phase separation

Christina Glen Robb[1], Thuy P. Dao[2], Jakub Ujma[3], Carlos A. Castañeda[2], Rebecca Beveridge[1]*

[1] Department of Pure and Applied Chemistry, University of Strathclyde, Glasgow, United Kingdom

[2] Departments of Biology and Chemistry; BioInspired Institute, Syracuse University, NY, USA

[3] Waters Corporation, Stamford Avenue, Altrincham Road, Wilmslow, United Kingdom

* Correspondence: rebecca.beveridge@strath.ac.uk

Abstract

Liquid-liquid phase separation (LLPS) is a process by which proteins and macromolecules condense into a dense phase that resembles liquid droplets. Ubiquilin-2 (UBQLN2), a ubiquitin (Ub)-binding protein with intrinsically disordered regions, undergoes LLPS alone under physiological conditions and colocalises with stress granules, which are a type of membraneless organelle hypothesised to form via phase separation. LLPS of UBQLN2 is driven by high salt concentration and reversed by the presence of Ub. However, the effects that these conditions have on the overall conformation of UBQLN2 remain unknown. Using ion mobility mass spectrometry (IM-MS), we discovered that UBQLN2 exists as a mixture of monomers and dimers, and that increasing salt concentration causes the UBQLN2 dimers to undergo a subtle shift towards extended conformations. In the presence of Ub, we observed 2:1 and 2:2 UBQLN2:Ub complexes which have compact geometries compared to free UBQLN2 dimers. Together, these data suggest that extended conformations of UBQLN2 are correlated with the ability of UBQLN2 to phase separate. Overall, delineating the conformations that are implicit in LLPS will greatly increase understanding of the process, both in normal cell physiology and in disease states such as in amyotrophic lateral sclerosis that can be caused by mutations to UBQLN2. This work demonstrates the strength of IM-MS in uncovering the molecular mechanisms of LLPS using full-length protein constructs.

Introduction

Intrinsically disordered proteins (IDPs) exist and function without the fixed tertiary structure that was once thought to be required for all proteins to carry out their physiological roles. Instead, IDPs populate a wide range of conformations, from compact to extended, and rapidly interconvert between these various geometries largely unhindered by energetic constraints [1]. IDPs and intrinsically-disordered regions (IDRs) in proteins are an important focus of research as 30% of the human proteome is predicted to be disordered [2]. Dysregulation of IDP biophysical properties is often associated with diseases such as cancer and neurodegenerative disorders as a result of IDP involvement in cell signalling networks [3, 4]. Additionally, long IDRs are often involved in multivalent interactions that contribute to liquid-liquid phase separation (LLPS), hypothesised to underlie formation of biomolecular condensates [5-7]. LLPS is important in normal cell physiology, and dysfunctional LLPS is involved in diseases such as amyotrophic lateral sclerosis (ALS) [8].

Ubiquitin (Ub)-binding proteasomal shuttle Ubiquilin-2 (UBQLN2) is an ALS-linked, IDR-containing protein that undergoes LLPS under physiological conditions [9-12]. UBQLN2 phase separation is modulated by multivalent interactions among IDRs that include the STI1-II region and disease-associated PXX domain [11-14], as well as the folded N-terminal Ub-like (UBL) and C-terminal Ub-associating (UBA) domains that bind proteasomal subunits [15] and Ub/polyUb chains [16], respectively (Figure 1a, b). The STI1-II region drives protein oligomerisation that is a prerequisite for UBQLN2 phase separation [10, 12]. UBQLN2 phase separation occurs in response to increases in salt concentration and temperature [17]. Importantly, noncovalent interactions between monoUb and the UBA domain of UBQLN2 inhibit the formation of the UBQLN2 droplets by disrupting the protein-protein interactions that drive LLPS [10]. We hypothesise that the promotion or inhibition of UBQLN2 LLPS result from changes in the global UBQLN2 conformation which is sensitive to salt concentration, temperature, and Ub-binding. However, UBQLN2 conformations under these different conditions remain elusive to most biophysical techniques (small angle X-ray scattering (SAXS), analytical ultracentrifugation (AUC), and nuclear magnetic resonance (NMR)) as these methods require high protein concentrations at which UBQLN2 phase separates. Furthermore, the combination of high IDR content and oligomerisation propensity of UBQLN2 complicates interpretation of experiments that inform on conformation [10, 11].

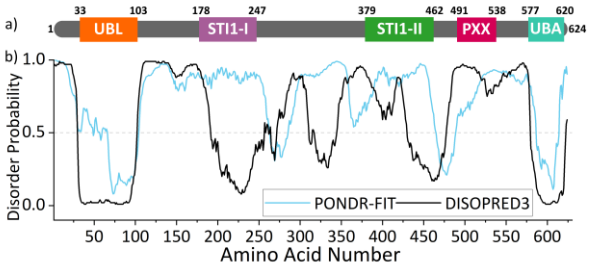

Figure 1. (a) Domain architecture of UBQLN2. (b) PONDR-FIT and DISOPRED3 predictions of disorder for UBQLN2, showing that the UBL and UBA are structured, with the region between being largely disordered. Figure adapted from Dao et al. [10].

Native mass spectrometry (nMS) and ion mobility mass spectrometry (IM-MS) have emerged as versatile and informative methods to study IDPs and proteins containing IDRs [18, 19]. Upon "soft" transfer from solution into the gas phase by nanoelectrospray ionisation (nESI), non-covalent interactions within and between proteins can be preserved, enabling the mass-to-charge ratio (*m/z*) measurement of intact proteins and protein complexes. Deconvolution of nMS data reveals the stoichiometric composition of a protein complex (*via* mass, *m*), and the degree of compaction or extension of a protein/protein complex can be correlated with a number of associated charges, *z* [20]. Compact conformations have a limited solvent accessible surface area on which protons can be accommodated, and hence have a low number of charges, whereas extended conformations have space to accommodate a large number of protons and therefore have a high charge state [21]. The wide charge state distribution, which is a hallmark of IDPs in nMS experiments, reflects their wide range of adopted conformations.

The hybrid method of IM-MS adds an extra dimension of analysis by separating protein ions on the basis of their overall size, meaning that multiple conformations can be separated from one *m/z* ratio. Larger conformations travel slower through an IM drift region, due to increased number of collisions with gas molecules [22]. The experiment yields arrival time distributions (ATDs) which can be converted to rotationally averaged collisional cross sections (CCSs) using appropriate calibrant proteins with known CCS values, to report on the size of the proteins of interest in units of nm^2 [23]. IM-MS therefore provides information on the range of sizes that a protein can exist in, which infers on their conformational ranges and hence their dynamic behaviour [24]. Advantages of using IM-MS to study IDPs include its ability to measure the size range of every species that is present in a stoichiometric mixture, including co-existing conformations of the same species, without any averaging over time and without interference from other complexes that are present in the mixture. Low protein concentrations are required, and the method is equally suited to compact and extended conformations and does not favour the folded state of a protein [20]. nMS and IM-MS have been

widely employed to study disordered protein systems such as p27 [21], α-synuclein [25] and melanoma-associated antigen A4 (MAGE-A4) [26]. IM-MS was also recently used to study the conformations of phase-separating proteins Fused in Sarcoma (FUS) and Transactive Response DNA-binding protein (TDP-43) in response to differing pH of the solution from which they were sprayed [27].

In this work, we used IM-MS to measure the conformational distributions of UBQLN2 in its soluble form, delineate its conformational response to increased salt concentration that drives LLPS, and interrogate the complexes it forms with Ub which reverses and inhibits LLPS. We identified that UBQLN2 exists as a mixture of monomers and dimers, both with an extraordinarily wide range of conformations. At increased salt concentration, the dimers undergo a subtle shift to more extended conformations which we hypothesise are implicit in driving LLPS. In contrast, the presence of Ub stabilises compact conformations of UBQLN2 dimers which we propose are unable to form the multivalent intermolecular interactions required for LLPS. These findings were enabled by the ability of IM-MS to (i) measure full-length UBQLN2 proteins, (ii) report on the conformations of individual complexes that are present in a mixture, and (iii) perform measurements at protein concentrations below the threshold for LLPS. These IM-MS experiments therefore reveal conformational changes associated with LLPS whilst retaining UBQLN2 in its soluble state.

Methods

Materials Ammonium acetate solution (AmAc) was prepared at pH 6.8 from ultra-pure water (18.2 MΩ.cm, Millipore) and analytical grade ammonium acetate solid. (Fisher Scientific).

Expression and purification of UBQLN2 and Ub

Full length (FL)-UBQLN2, UBQLN2-ΔUBA and ubiquitin (Ub) were expressed in *E. coli* NiCo21 (DE3) (New England BioLabs) cells in Luria-Bertani (LB) broth at 37°C overnight. Bacteria were pelleted, frozen, and lysed in 50 mM Tris pH 8, 1 mM EDTA, 1 mM PMSF, 4 mM $MgCl_2$, lysozyme and nuclease (ThermoFisher). For full-length UBQLN2 and UBQLN2-ΔUBA, NaCl was added to the cleared lysate at 30° C to the final concentrations of 0.5 M and 1 M, respectively, to induce UBQLN2 phase separation. UBQLN2 droplets were pelleted and then resuspended in 20 mM NaPhosphate, 0.5 mM EDTA, 0.1 mM TCEP, 0.02% NaN_3 (pH 6.8). Leftover NaCl was removed through HiTrap desalting column (GE Healthcare). For Ub, perchloric acid was added to the lysate to a final pH of about 1. Precipitated proteins were cleared by centrifugation. The supernatant was diluted 1:1 with 50 mM AmAc, pH 4.5, loaded onto HiTrap SP HP column (GE Healthcare), and eluted with a gradient to 1 M NaCl in 50 mM AmAc, pH 4.5. Fractions containing Ub were concentrated and buffer exchanged into pH 6.8 buffer (see above) using Vivaspin 6 centrifugal concentrators with MWCO of 5000 Da (Sartorius). Purified proteins were frozen at −80°C.

Preparation of proteins for nMS and IM-MS Full length FL-UBQLN2 (30 µM) and UBQLN2-ΔUBA (45 µM) were buffer exchanged into 10 mM AmAc pH 6.8 using 96-well Microdialysis plates (Thermo Fisher Scientific, Waltham, MA USA). Ub was buffer exchanged using Bio-Rad Micro Bio-Spin P6 columns (Bio-Rad, Hercules, CA, USA). Final protein concentrations were determined using a NanoDrop spectrophotometer (Thermo Fisher Scientific Waltham, MA USA) using the A280 method.

Native mass spectrometry and ion mobility FL-UBQLN2 was diluted to a protein concentration of 15 µM and final AmAc concentrations of 10 mM, 50 mM, or 75 mM (pH 6.8) for experiments on the unbound protein. UBQLN2-ΔUBA was diluted to 5 µM, AmAc concentrations of 10 mM, 55 mM and 100 mM (pH 6.8). For experiments with FL-UBQLN2 and Ub, a 1:4 molar ratio of FL-UBQLN2 monomer to Ub was mixed by adding 15 µM FL-UBQLN2 (10 mM AmAc) to an equal volume of 60 µM Ub (10 mM AmAc). All samples were allowed to equilibrate on ice for at least 30 minutes.

Ion mobility mass spectrometry data was acquired on a Waters Synapt G2-Si (Waters Corporation, Wilmslow, UK) instrument operated in “Sensitivity” mode. Proteins were subject to nanoelectrospray ionisation (nESI) in positive mode with a nanospray tip pulled in-house with a Flaming/Brown P-97 micropipette puller from thin-walled glass capillaries (i.d. 0.78 mm, o.d. 1.0 mm, 10 cm length, both

from Sutter Instrument Co., Novato, CA, USA). A positive potential of 1.2-1.6 Kv was applied to the solution via a thin platinum wire. Other non-default instrument settings include: sampling cone voltage 60V, collision voltage 5V, trap gas flow 3.5-4 ml/min, source temperature 40 °C. Ion mobility data of FL-UBQLN2 alone and UBQLN2-ΔUBA was collected at travelling-wave velocity of 400 m/s and height of 40V. Ion mobility of UBQLN2:Ub complexes was collected at travelling-wave velocity of 325 m/s and ramped height of 25-40V. Helium and nitrogen (IMS) gas flows were 180 ml/min and 90 ml/min for experiments involving FL-UBQLN2 and UBQLN2-ΔUBA, and 150 and 75 ml/min for experiments involving FL-UBQLN2:Ub complexes. Instrument was allowed to settle for one hour prior to experiments. Quad RF profile was applied to improve transmission of ions from *m/z* 2750 and upwards. CCS calibration was performed using IMSCal19 (Waters Corporation, Wilmslow, UK) [23, 28] with β-lactoglobulin and bovine serum albumin used as CCS calibrants [29].

Data processing Mass spectra were initially processed in MassLynx v4.2 (Waters Corporation, Wilmslow, UK). IM-MS profiles were created in OriginPro 2022 (OriginLab Corporation, Northampton, MA, USA) by extracting ion mobility spectra from selected charge states in the mass spectrum, then normalising and averaging spectra collected from multiple tips, on the same day. For FL-UBQLN2, normalised data from across multiple days was then averaged and the standard deviation across multiple days was calculated using Descriptive Statistics function in OriginPro 2022 and reported as error bars. For UBQLN2-ΔUBA, data was collected in triplicate on one day and the standard deviation across measurements was calculated using Descriptive Statistics function in OriginPro 2022 and reported as error bars. Baseline subtraction was performed using Peak Analyser: Create baseline function in OriginPro2022 where anchor points along baseline were selected manually and connected using BSpline interpolation method. Text files generated from CCS calibration using IMSCal19 were collated in Microsoft Excel and scatter plots of CCS versus charge were plotted in OriginPro2022 by extracting the maxima(s) for each charge states' CCS values. Figures were created using Inkscape 1.2.1 (inkscape.org).

Bright-field imaging of phase separation Samples were prepared to contain 15 µM FL-UBQLN2 or 5-10 µM UBQLN2-ΔUBA and different concentrations of AmAc, pH 6.8 from 10 mM to 300 mM (FL-UBQLN2) and 10 to 400 mM (UBQLN2-ΔUBA), and incubated on ice. Samples were added to Eisco Labs Microscope Slides, with Single Concavity, and covered with MatTek coverslips that had been coated with 5% bovine serum albumin (BSA) to minimise changes due to surface interactions, and incubated coverslip-side down at 20 ºC for 10 min. Phase separation was imaged on an ONI Nanoimager (Oxford Nanoimaging Ltd, Oxford, UK) equipped with a Hamamatsu sCMOS ORCA flash 4.0 V3 camera using an Olympus 100×/1.4 N.A. objective. Images were prepared using Fiji [30] and FigureJ plugin.

Results and discussion

Delineating the effect of salt concentration on the mass spectrometry profile of FL-UBQLN2

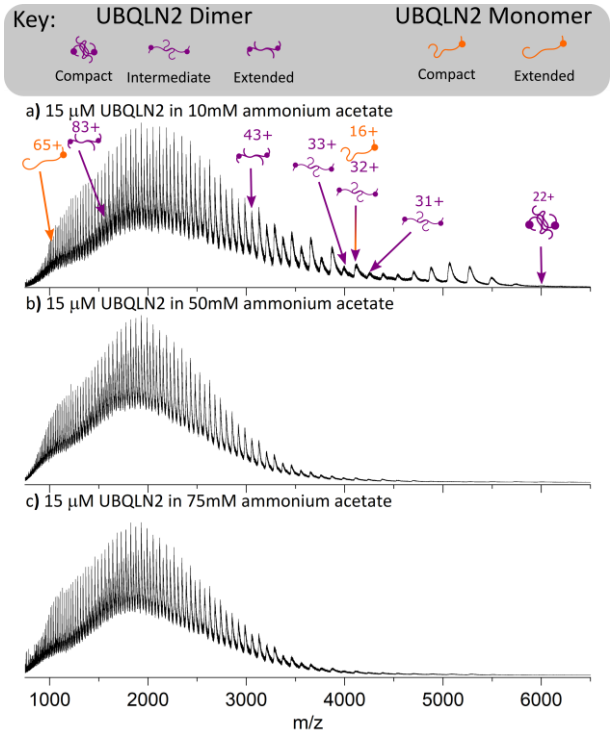

Figure 2. nMS reveals a loss of compact UBQLN2 dimers with increasing salt concentration. FL-UBQLN2 (15 µM monomer) is sprayed from AmAc concentrations of 10 mM (a), 50 mM (b) and 75 mM (c).

As increased salt concentration promotes UBQLN2 LLPS, our first objective was to determine the effect of changing salt concentration on the conformational ensemble of FL-UBQLN2 by spraying the protein from ammonium acetate (AmAc) concentrations of 10 mM, 50 mM and 75 mM representing low, medium and high salt concentrations, respectively. Whilst FL-UBQLN2 does not phase separate under these conditions, AmAc is capable of inducing LLPS at higher concentrations (Figure S1). When sprayed from the 10 mM salt solution (Figure 2a), FL-UBQLN2 exists as a mixture of monomers and dimers with the monomer present in charge states 16+ to 65+ (Δz=49) and the dimer present in charge states 22+ to 83+ (Δz=61). The measured mass of the monomer is 65 640 Da and that of the dimer is 131 280 Da. Both charge state distributions represent extremely dynamic species, as the maximum Δz of a structured protein was previously found to be 6 for proteins up to 150 kDa in mass [20]. We focus primarily on the dimeric species, as these undergo changes in response to solution conditions and we therefore assign these as being implicit in LLPS. We assign the low-charged dimers of charge states 22+ to 31+ (*m/z* 4200-5750) as compact, dimer charge states 32+ to 43+ (*m/z* 3000-4200) as being intermediate, and dimer charge states 44+ and above (*m/z* 750-3000) as being extended. At medium

and high AmAc concentrations (Figure 2b and c) the compact dimers have a much lower signal intensity. This suggests that increased salt concentration, which drives UBQLN2 LLPS, causes a decrease in the abundance of compact dimers. Of note, 75mM was the highest concentration of AmAc from which the protein could be sprayed without the nanoelectrospray needle becoming blocked by insoluble protein.

A construct of UBQLN2 lacking the UBA domain (UBQLN2-ΔUBA), which undergoes LLPS to a much lower degree than FL-UBQLN2 [10], was also subject to nMS analysis. After ascertaining that UBQLN2-ΔUBA remains soluble in AmAc concentrations of up to 400 mM (Figure S2), we sprayed UBQLN2-ΔUBA from AmAc concentrations of 10 mM, 55 mM and 100 mM (Figure S3). This construct follows the same trend as FL-UBQLN2 in that low charge states, corresponding to compact conformations, are represented to a much lower extent at higher AmAc concentrations. In this case, whilst the most intense monomer peak switches from 31+ to 52+ as salt concentration increases, the most intense dimer peak remains at 69+ throughout (Figure S3). Therefore, these UBQLN2-ΔUBA data are consistent with the elongation of FL-UBQLN2 observed with increased salt concentration being an intermediate step towards LLPS, rather than what remains soluble after LLPS of a different conformation has taken place.

Ion mobility mass spectrometry reveals elongation of intermediate dimer conformations at increasing salt concentrations

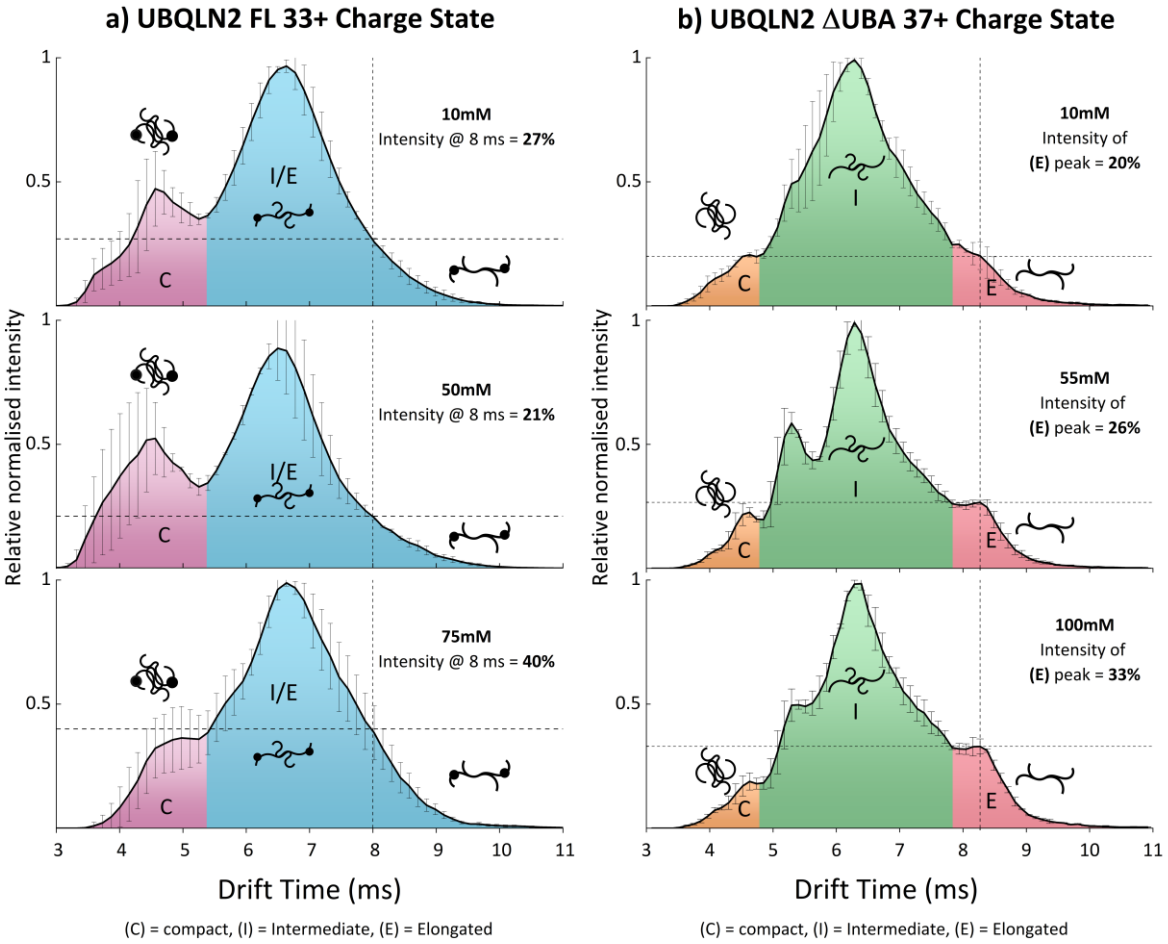

Figure 3. IM-MS shows that the intermediate dimer conformations of FL-UBQLN2 and UBQLN2-ΔUBA become larger when sprayed from high salt concentrations. (a) IM spectra of the FL-UBQLN2 33+ dimer sprayed from AmAc concentrations of 10 mM (top), 50 mM (middle) and 75 mM (bottom). (b) IM spectra of the UBQLN2-ΔUBA 37+ dimer sprayed from AmAc concentrations of 10 mM (top), 55 mM (middle) and 100 mM (bottom). Solid black line in figure 3a is the average of 3 measurements across three days (n=9) and error bars represent standard deviation across days. Solid black line in figure 3b is the average of n=3 measurements taken on one day and error bars represent standard deviation across measurements. Horizontal dashed line represents the signal intensity at 8 ms in (a) and 8.2 ms (b) which corresponds to the most extended dimers.

IM-MS was subsequently used to investigate whether UBQLN2 undergoes conformational changes upon increasing the concentration of AmAc in the starting solution. The high charge states corresponding to elongated conformations remain unaffected (47+ dimer, Figure S4). While the

compact conformations couldn't be compared as the signal intensity for medium and high salt concentrations were too low, arrival time distributions (ATDs) shown for charge states 24+ to 30+ in 10mM AmAc (Figure S5) confirm that FL-UBQLN2 at charge states 24+ to 27+ are mainly compact, and then become more elongated between 28+ and 30+. The intermediate dimer populations underwent a subtle shift towards more elongated conformations with increases in salt concentration, represented by the peak corresponding to the 33+ dimer (*m/z* 3975, Figure 3a) of FL-UBQLN2, as described below.

The ATDs of the FL-UBQLN2 33+ dimer sprayed from low, medium and high AmAc concentrations are shown in Figure 3a. When sprayed from low and medium AmAc there is a bimodal ATD in which peak I has an apex of 4.6 ms and is attributed to compact dimer conformations, and peak II has an apex of 6.6 ms and is attributed to intermediate and extended dimer conformations. At high AmAc, the relative intensity of peak I is reduced to ~35% from ~50% and is a shoulder to Peak II rather than being a separately resolved peak as at 10 mM and 50 mM AmAc. Overall, this shows the compact conformations of the FL-UBQLN2 33+ dimer at 75mM AmAc are in lower abundance and have longer drift times, compared to 10mM and 50mM AmAc.

Whilst the apex of peak II remains largely unchanged as AmAc concentration is increased, there is a higher signal intensity at drift times above 8 ms when FL-UBQLN2 is sprayed from 75 mM AmAc (40% c.f. 27% and 21% for 10 mM and 50 mM, respectively), indicating that there is a higher abundance of more elongated conformations at high salt concentrations that drive LLPS. ATDs for the overlapping 32+dimer/ 16+ monomer are shown in Figure S6 which shows that the conformation of the 16+ monomer is largely unaffected by increasing AmAc concentrations.

ATDs of the 37+ charge state of UBQLN2-ΔUBA were also compared when sprayed from 10mM, 55mM and 100mM AmAc (Figure 3b). At 10mM, the ATD is broad and relatively featureless, indicating rapid, unhindered interconversion between many conformational families. At 55 mM and 100 mM AmAc, a compact conformational family is resolved (apex 4.6 ms), along with two intermediate conformational families (apex 5.3 and 6.3 ms) and an extended conformational family (8.2 ms). Again, the extended conformation increases in intensity as AmAc concentration increases. We envision that an extended conformation of FL-UBQLN2 is also becoming more intense at high AmAc, but in this case the conformation is not resolvable in the ATD due to increased dynamics of the system.

UBQLN2 binds to Ub in 2:1 and 2:2 complexes which stabilises compact conformations

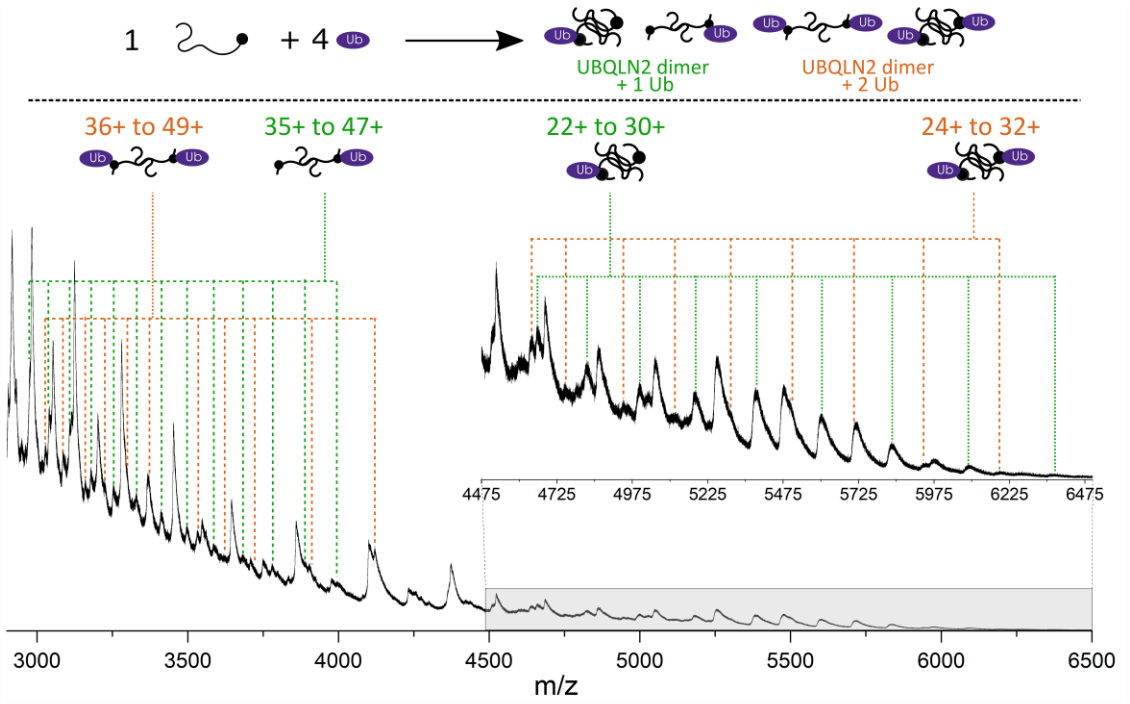

Figure 4: Native mass spectrum (2900-6500 *m/z*) resulting from a 1:4 molar ratio of FL-UBQLN2:Ub in 10 mM AmAc. Mixture results in the formation of 2:1 (green) and 2:2 (orange) FL-UBQLN2 to Ub complexes.

As specific interactions between UBQLN2 and Ub (monoUb) drive disassembly of UBQLN2 biomolecular condensates [10], we used nMS to investigate the stoichiometry and conformation of the FL-UBQLN2:Ub complexes. The native mass spectrum of a 1:4 molar ratio of UBQLN2 monomer to Ub reveals that Ub binds to UBQLN2 dimers with either 2:1 or 2:2 UBQLN2 to Ub stoichiometry (Figure 4). The measured mass of the 2:1 complex is 139 820 Da and that of the 2:2 complex is 148 440 Da. Charge states for the 2:1 complex, labelled with green dotted lines, range from 22+ to 47+, with charge states 30+ to 35+ being much lower in intensity and not resolved from other peaks in the same *m/z* range (Figure S7). Complexes with 2:2 stoichiometry labelled with orange dotted lines, range from 24+ to 49+ with a gap in resolvable peaks from 33+ to 39+, as well at 41+ and 43+, and are lower in intensity than the 2:1 complexes. Whilst monomeric UBQLN2 is not observed to bind to Ub, this cannot be ruled out due to the overlapping *m/z* values between the 1:1 complex and evenly charged 2:2 complex. However, no increase in abundance of the evenly charged 2:2 complexes is observed compared to the oddly charged, which would be the indication of 1:1 complex. Moreover, signal corresponding to monomeric UBQLN2 remains at high intensity in the mixture with Ub, indicating that it is still present in solution, whereas the signal intensity for unbound UBQLN2 dimers is depleted as it complexes with Ub.

The charge state range of both Ub-containing complexes (Δz = 25 in both cases) is much narrower than the range observed for FL-UBQLN2 alone (Δz = 61) but is still very wide compared to a structured protein of a similar size (Δz = 6 for Serum Amyloid P Pentamer, 128 kDa [20]), suggesting the complexes are still highly dynamic. A comparison of the nMS of UBQLN2 and UBQLN2:Ub complexes can be seen in Figure S7. Another feature of the mass spectrum worth noting is the reduction in intensity of the peaks previously assigned as intermediate-charged UBQLN2 dimers (3000-4200 *m/z*), indicating that these are the dimeric charge states that are binding to Ub and are therefore of lower abundance in solution. These also correspond to the charge states which form elongated conformations in response to salt concentration (Figure 3). We hypothesise these are the conformations that are responsive to variations in solution conditions and mediate LLPS of UBQLN2.

As mentioned previously, it is possible to convert drift time values collected in IM-MS experiments to rotationally averaged collisional cross sections (CCS) using calibrant proteins with known CCS values [23, 28]. This has been performed for UBQLN2 and UBQLN2:Ub complexes to allow comparison of sizes between different UBQLN2 complexes.

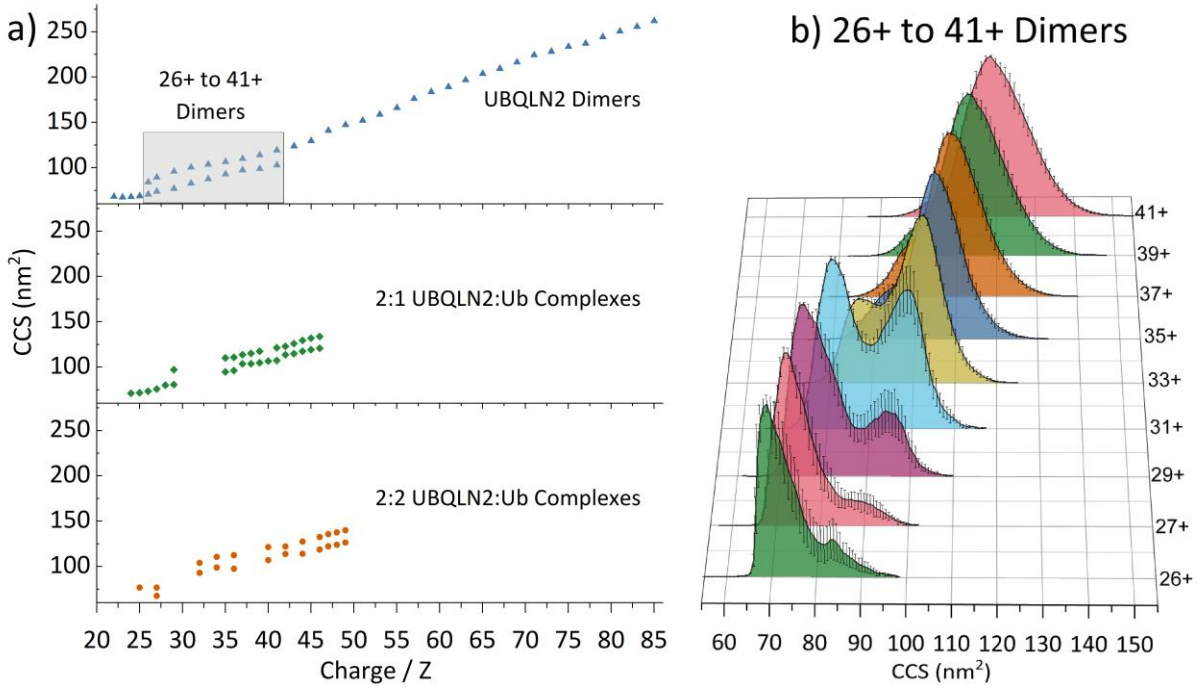

Figure 5: a) Collision cross section distributions of UBQLN2 dimers, UBQLN2:Ub 2:1 complexes and 2:2 complexes. b) Calibrated collisional cross section distributions for free UBQLN2 dimer charge states 26+ to 41+. A bimodal distribution can be observed wherein the compact conformation dominates from 26+ to 31+ until a conformational switch occurs and the more elongated conformation dominates from 35+, trending larger as charge increases. Solid black line represents

average from three measurements and error bars represent standard deviation across three measurements.

Figure 5a shows the CCS values for individual charge states of UBQLN2 dimers and 2:1 and 2:2 UBQLN2:Ub complexes. For the UBQLN2 dimers, only odd charge states are shown above 31+ to avoid interference of signal from the monomer. For UBQLN2:Ub complexes, charge states which are not calibrated are marked with red crosses in figure S7. Charge states 22+ to 25+ exist in a single compact conformational family around 68 nm^2, while charge states 26+ to 41+ exist in two conformational families shown by a bimodal ATD for these charge states (Figure 5b). Charge states 43+ to 85+ correspond to a conformational family that increases in size with increasing charge, typical of IDPs. Overall, UBQLN2 dimers range from 68 to 260 nm^2, which is a huge range of conformations for a complex of this mass. For reference, the Serum Amyloid P Pentamer (128 kDa) has a CCS range of 59-64 nm^2 [20].

UBQLN2:Ub complexes are present in a smaller range of CCSs, indicating that Ub stabilises compact conformations of UBQLN2, with the largest conformation in both cases being ~135 nm^2 as opposed to 260 nm^2 for the UBQLN2 dimer. For the 2:1 UBQLN2:Ub complex, a compact conformational family exists from 71-80 nm^2 (charge states 24+ to 29+). 29+ has two conformational families at 80 and 98 nm^2, then there is a gap in resolvable *m/z* peaks from 30+ to 34+ (Figure S7, red crosses). From 35+ to 47+ the large conformation increases in size gradually with CCSs from 110-132 nm^2, whilst the smaller conformation of these charge states has slightly larger changes in CCS between charge states 36+ to 37+ and 42+ to 43+.

The 2:2 UBQLN2:Ub complexes follow a similar trend, in which compact complexes exist at CCSs of 68-76 nm^2 (z = 25+ to 27+), there is then a gap in resolvable *m/z* peaks (CCS 78-92 nm^2, z = 27+ to 31+) and from z = 32+ to 49+ there are two conformations per charge state, with an overall increase in CCS with respect to charge. Not shown in this region are charge states z = 37+ to 39+, CCS 107-112 nm^2, as they are poorly resolved and in low abundance. The largest CCS for the 2:2 complex is marginally larger than the 2:1 complex: 140 vs 135 nm^2. We were interested to note that the most compact conformations of the UBQLN2:Ub complexes have similar CCS values to the most compact UBQLN2 dimers despite the increase in mass, suggesting that addition of ubiquitin is stabilising even more compact conformations of UBQLN2 than the free UBQLN2 dimers. Additionally, the complexes with Ub do not reach the size of the most extended conformations for free UBQLN2 dimers. When considering LLPS, this could mean addition of ubiquitin is preventing UBQLN2 inter-molecular interactions by stabilising compact conformations.

Conclusions

In this work, we demonstrated the strength of nMS and IM-MS in elucidating conformational details of UBQLN2 in conditions where LLPS is promoted (high salt concentration) and inhibited (presence of Ub) (Figure 6). We found that LLPS-promoting high salt concentration depletes compact conformations and causes a subtle shift of UBQLN2 towards more elongated conformations. Conversely, Ub, which inhibits and reverses LLPS of UBQLN2, binds to and favours more compact conformations of UBQLN2 dimers.

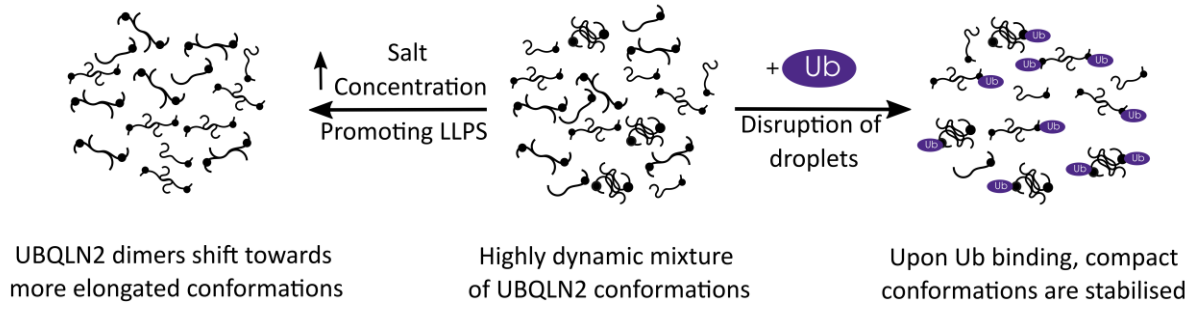

Figure 6: Model of changes in full-length UBQLN2 conformational state as a function of LLPS-promoting (salt addition) and LLPS-inhibiting (monoUb addition) conditions.

Determination of how conformation contributes to LLPS of specific proteins has been hampered by the challenges corresponding to alternative biophysical methods to measure conformational disparity. These include the size limitation in NMR experiments, the high protein concentrations required for methods such as NMR and AUC, and the inability of many methods to differentiate multiple complexes present in a mixture. We present nMS and IM-MS as versatile, label-free methods to individually measure several complexes in a mixture. These methods reveal subtle shifts in protein conformations that result from alterations in the solution conditions from which they are sprayed. A strong advantage of these MS methods is the sensitivity: proteins can be measured at low concentrations below the threshold for LLPS, thereby delineating conformational changes that occur *en route* to droplet formation.

The strength of MS in determining the underlying mechanisms of LLPS has been highlighted in two recent publications. Sahin et al. [27] used nMS and IM-MS to measure the conformations of engineered FUS and TDP-43 constructs that contain a spider silk domain for solubility. These proteins undergo LLPS at neutral pH but remain soluble at high pH, allowing the authors to track changes in conformation as they reduce the pH and move towards LLPS conditions. They observed that FUS

undergoes an unfolded-to-globular transition as the pH is shifted from 12.5 to 7, which they attribute to conformational changes associated with LLPS, whereas TDP-43 oligomerises into partially disordered dimers and trimers. Ubbiali et al. [31] used crosslinking-MS to investigate the conformations of the IDP α-Synuclein under LLPS conditions, and discovered that α-Synuclein shifts towards more elongated conformations, making it amenable to interprotein interactions. This agrees with our assertions about UBQLN2, and we propose that elongation may be a common factor in the LLPS of IDPs, as it allows the formation of multivalent long-range interactions among protein molecules.

Our findings about the mechanism of LLPS of UBQLN2 have allowed us to speculate on how this affects the function of the protein *in vivo*. We propose that when UBQLN2 is in its free, unbound state, it is present in elongated conformations. This enables UBQLN2 to interact with other UBQLN2 molecules via the multivalent interactions involving the folded and disordered regions that promote its phase separation [10, 17]. Additionally, these interactions may include other protein components such as RNA-binding proteins that are found in stress granules and known to interact with UBQLN2 [32, 33]. Upon binding ubiquitin, we speculate that interactions within and between UBQLN2 dimers are disrupted, resulting in more compact conformations of UBQLN2 that do not favour phase separation. In this way, noncovalent interactions between UBQLN2 and monoubiquitinated substrates can potentially drive disassembly of UBQLN2 droplets or remove UBQLN2 from condensates inside cells. This research, in the future, will aid in determining how the conformational states of UBQLN2 are affected by ALS-linked mutations as well as engagement with other protein quality control components such as polyubiquitin chains and proteasomal receptors.

Acknowledgements

RB is supported by a UKRI Future Leaders Fellowship (Grant Reference MR/T020970/1) and a Chancellor's Fellowship from the University of Strathclyde. CGR acknowledges funding from Waters Corporation (UK). T.P.D. and C.A.C. are supported by NSF CAREER (MCB 1750462). We also acknowledge Magnus Kjaergaard and Alex Holehouse of IDPseminars for introducing the authors and initiating this fruitful collaboration!

Conflict of interest statement

J.U. is an employee of Waters Corporation (Wilmslow, UK) who manufactures and sells IM-MS instrumentation.

Data availability

All raw data are attached as supplementary files.

References

1. Wright, P.E. and H.J. Dyson, *Intrinsically disordered proteins in cellular signalling and regulation.* Nat Rev Mol Cell Biol, 2015. **16**(1): p. 18-29.
2. Leuenberger, P., et al., *Cell-wide analysis of protein thermal unfolding reveals determinants of thermostability.* Science, 2017. **355**(6327): p. eaai7825.
3. Uversky, V.N., C.J. Oldfield, and A.K. Dunker, *Intrinsically disordered proteins in human diseases: introducing the D2 concept.* Annu Rev Biophys, 2008. **37**: p. 215-46.
4. Uversky, V.N., *Intrinsically Disordered Proteins*, in *Structural Biology in Drug Discovery*. 2020. p. 587-612.
5. Choi, J.-M., A.S. Holehouse, and R.V. Pappu, *Physical Principles Underlying the Complex Biology of Intracellular Phase Transitions.* Annual Review of Biophysics, 2020. **49**(1): p. 107-133.
6. Banani, S.F., et al., *Biomolecular condensates: organizers of cellular biochemistry.* Nature Reviews Molecular Cell Biology, 2017. **18**(5): p. 285-298.
7. Shin, Y. and C.P. Brangwynne, *Liquid phase condensation in cell physiology and disease.* Science, 2017. **357**(6357): p. eaaf4382.
8. Renaud, L., et al., *Key role of UBQLN2 in pathogenesis of amyotrophic lateral sclerosis and frontotemporal dementia.* Acta Neuropathologica Communications, 2019. **7**(1): p. 103.
9. Grice, G.L. and J.A. Nathan, *The recognition of ubiquitinated proteins by the proteasome.* Cell Mol Life Sci, 2016. **73**(18): p. 3497-506.
10. Dao, T.P., et al., *Ubiquitin Modulates Liquid-Liquid Phase Separation of UBQLN2 via Disruption of Multivalent Interactions.* Mol Cell, 2018. **69**(6): p. 965-978.e6.
11. Dao, T.P., et al., *ALS-Linked Mutations Affect UBQLN2 Oligomerization and Phase Separation in a Position- and Amino Acid-Dependent Manner.* Structure, 2019. **27**(6): p. 937-951.e5.
12. Riley, J.F., et al., *ALS-linked mutations impair UBQLN2 stress-induced biomolecular condensate assembly in cells.* J Neurochem, 2021. **159**(1): p. 145-155.
13. Hjerpe, R., et al., *UBQLN2 Mediates Autophagy-Independent Protein Aggregate Clearance by the Proteasome.* Cell, 2016. **166**(4): p. 935-949.
14. Ford, D.L. and M.J. Monteiro, *Dimerization of ubiquilin is dependent upon the central region of the protein: evidence that the monomer, but not the dimer, is involved in binding presenilins.* Biochem J, 2006. **399**(3): p. 397-404.
15. Ko, H.S., et al., *Ubiquilin interacts with ubiquitylated proteins and proteasome through its ubiquitin-associated and ubiquitin-like domains.* FEBS Lett, 2004. **566**(1-3): p. 110-4.
16. Zhang, D., S. Raasi, and D. Fushman, *Affinity makes the difference: nonselective interaction of the UBA domain of Ubiquilin-1 with monomeric ubiquitin and polyubiquitin chains.* J Mol Biol, 2008. **377**(1): p. 162-80.
17. Zheng, T., S.K.K. Galagedera, and C.A. Castañeda, *Previously uncharacterized interactions between the folded and intrinsically disordered domains impart asymmetric effects on UBQLN2 phase separation.* Protein Sci, 2021. **30**(7): p. 1467-1481.
18. Beveridge, R. and A.N. Calabrese, *Structural Proteomics Methods to Interrogate the Conformations and Dynamics of Intrinsically Disordered Proteins.* Frontiers in Chemistry, 2021. **9**.
19. Santambrogio, C., E. Ponzini, and R. Grandori, *Native mass spectrometry for the investigation of protein structural (dis)order.* Biochim Biophys Acta Proteins Proteom, 2022. **1870**(10): p. 140828.
20. Beveridge, R., et al., *A Mass-Spectrometry-Based Framework To Define the Extent of Disorder in Proteins.* Analytical Chemistry, 2014. **86**(22): p. 10979-10991.

21. Beveridge, R., et al., *Ion Mobility Mass Spectrometry Uncovers the Impact of the Patterning of Oppositely Charged Residues on the Conformational Distributions of Intrinsically Disordered Proteins.* Journal of the American Chemical Society, 2019. **141**(12): p. 4908-4918.
22. Gabelica, V. and E. Marklund, *Fundamentals of ion mobility spectrometry.* Current Opinion in Chemical Biology, 2018. **42**: p. 51-59.
23. Bush, M.F., et al., *Collision Cross Sections of Proteins and Their Complexes: A Calibration Framework and Database for Gas-Phase Structural Biology.* Analytical Chemistry, 2010. **82**(22): p. 9557-9565.
24. Eldrid, C., et al., *Cyclic Ion Mobility–Collision Activation Experiments Elucidate Protein Behavior in the Gas Phase.* Journal of the American Society for Mass Spectrometry, 2021. **32**(6): p. 1545-1552.
25. Moons, R., et al., *Effects of Detergent on α-Synuclein Structure: A Native MS-Ion Mobility Study.* International Journal of Molecular Sciences, 2020. **21**(21): p. 7884.
26. Hagiwara, Y., et al., *Consequences of point mutations in melanoma-associated antigen 4 (MAGE-A4) protein: Insights from structural and biophysical studies.* Scientific Reports, 2016. **6**(1): p. 25182.
27. Sahin, C., et al., *Mass spectrometry of RNA-binding proteins during liquid-liquid phase separation reveals distinct assembly mechanisms and droplet architectures.* bioRxiv, 2022: p. 2022.09.28.509878.
28. Richardson, K., et al., *An Improved Calibration Approach for Traveling Wave Ion Mobility Spectrometry: Robust, High-Precision Collision Cross Sections.* Analytical Chemistry, 2021. **93**(7): p. 3542-3550.
29. Allen, S.J., A.M. Schwartz, and M.F. Bush, *Effects of Polarity on the Structures and Charge States of Native-Like Proteins and Protein Complexes in the Gas Phase.* Analytical Chemistry, 2013. **85**(24): p. 12055-12061.
30. Schindelin, J., et al., *Fiji: an open-source platform for biological-image analysis.* Nat Methods, 2012. **9**(7): p. 676-82.
31. Ubbiali, D., et al., *Direct Observation of "Elongated" Conformational States in α-Synuclein upon Liquid-Liquid Phase Separation.* Angewandte Chemie International Edition. **n/a**(n/a): p. e202205726.
32. Cassel, J.A. and A.B. Reitz, *Ubiquilin-2 (UBQLN2) binds with high affinity to the C-terminal region of TDP-43 and modulates TDP-43 levels in H4 cells: Characterization of inhibition by nucleic acids and 4-aminoquinolines.* Biochimica et Biophysica Acta (BBA) - Proteins and Proteomics, 2013. **1834**(6): p. 964-971.
33. Gilpin, K.M., L. Chang, and M.J. Monteiro, *ALS-linked mutations in ubiquilin-2 or hnRNPA1 reduce interaction between ubiquilin-2 and hnRNPA1.* Human Molecular Genetics, 2015. **24**(9): p. 2565-2577.